Ballistic Electron Emission Microscopy on $CoSi_2$/Si(111) interfaces: band structure induced atomic-scale resolution and role of localized surface states

K. Reuter[1,3], F.J. Garcia-Vidal[2], P.L. de Andres[1], F. Flores[2], and K. Heinz[3]
[1]*Instituto de Ciencia de Materiales (CSIC), Cantoblanco, E-28049 Madrid (Spain)*
[2]*Departamento de Física Teórica de la Materia Condensada (UAM) E-28049 Madrid (Spain)*
[3]*Lehrstuhl für Festkörperphysik, Universität Erlangen-Nürnberg, Staudtstr. 7, 91058 Erlangen (Germany)*
(February 7, 2008)

Applying a Keldysh Green's function method it is shown that hot electrons injected from a STM-tip into a $CoSi_2$/Si(111) system form a highly focused beam due to the silicide band structure. This explains the atomic resolution obtained in recent Ballistic Electron Emission Microscopy (BEEM) experiments. Localized surface states in the (2×1)-reconstruction are found to be responsible for the also reported anticorrugation of the BEEM current. These results clearly demonstrate the importance of bulk and surface band structure effects for a detailed understanding of BEEM data.

PACS numbers: 61.16.Ch, 72.10.Bg, 73.20.At

Ballistic Electron Emission Microscopy (BEEM), and its spectroscopic counterpart (BEES), are powerful techniques invented for exploring the electronic properties of metal-semiconductor (M-S) interfaces [1]. Thin metallic films are deposited on different semiconductor materials and the BEEM current, i.e. the current arriving at the semiconductor after injection into the metal surface from a Scanning Tunneling Microscope (STM) tip, is measured as a function of the tip-metal voltage [2]. The interpretation of these experiments is based on a three-step model: (i) first, electrons are injected from the tip into the metal (tunneling); (ii) then, electrons propagate through the film suffering collisions with different quasiparticles (transport), and (iii) finally, electrons overcome the Schottky barrier and enter into the semiconductor (matching of metal and semiconductor wavefunctions across the interface). The difficulty in analyzing experimental BEEM data stems from the strong influence of all three steps requiring a careful theoretical modeling to avoid spurious correlations between the parameters involved. Recently, it has been shown that the electronic band structure of the metal, which had been completely neglected in earlier free electron models, plays a crucial role in this regards [3].

Recent experimental BEEM investigations on metallic silicide films deposited on Si show (i) an atomic scale resolution of the M-S interface [4], and (ii) a striking dependence of the interface BEEM current on the silicide surface topography [5]. Dislocations and point defects at the interface were well visible giving direct access to its quality. This is rather important in view of the interface's role in building the Schottky barrier or with respect to the growth mode of silicides which are promising materials for microelectronic applications [6]. Equally important is the quantitative understanding of how the obtained atomic scale resolution is produced and why the BEEM current is related to the surface topography. In this paper, we show that the high lateral resolution is caused by the silicide's band structure, which in the case of $CoSi_2$/Si(111), on which we concentrate, makes the electrons focus in the <111> direction. This tells that the experimentally observed focusing is an intrinsic feature of such films that might be exploited in future applications. Additionally, the introduction of the appropriate surface electronic structure explains the BEEM current dependence on the tip position mainly as a result of the weight of localized surface states on the reconstructed surface.

We use a full quantum-mechanical description of the BEEM problem based on a Keldysh Green's function method [3]. This formalism presents the important advantage over standard E-space Monte-Carlo approaches of yielding an appropriate description of the electronic band structure. Moreover, inelastic effects associated with electron-electron interactions are also included in our method by adding a positive imaginary part to the energy of the electron. In order to analyze the first two steps of the BEEM process, we choose a local orbital basis for the description of the electronic structure of the tip and sample and the coupling between them. In particular, for $CoSi_2$ we use a slight modification of the tight-binding parameters given in [7], that accurately reproduce the band structure of this silicide around the Fermi level [8]. For the analysis of the interaction between tip and sample we assume that only the last atom in the tip (0) is connected to the sample. Hence, we express the coupling tip-sample in terms of a set of hopping matrices $\hat{T}_{0m}$, that link the tip atom (0) with the atom (m) in the sample surface. For each $\hat{T}_{0m}$, a WKB derived exponential damping is applied, valid because the tip-sample distance in BEEM is rather large.

Being interested in understanding the observed nanometric spatial resolution of this technique, we first analyze currents in real space. Within our formalism, the current between two sites i and j in the metal can be obtained from the following formula [3,9]:

$$J_{ij}(V) = \frac{4e}{\hbar} \Im \int_{eV_o}^{eV} Tr \sum_{mn} \left[\hat{T}_{ij} \hat{g}^R_{jm} \hat{T}_{m0} \hat{\rho}_{00} \hat{T}_{0n} \hat{g}^A_{ni} \right] dE, \quad (1)$$

where $\hat{T}_{ij}$ is the hopping matrix linking local orbitals of both sites (i and j), and the trace denotes summation over these orbitals. $\hat{g}^R_{jm}(E)$ is the retarded Green's function for the surface decoupled from the tip. This function describes the propagation of an electron between atoms j and m inside the metal, including the effect of the surface. Atom m in Eq. (1) is coupled to the tip atom 0 by a hopping matrix $\hat{T}_{m0}$, and $\hat{\rho}_{00}(E)$ is the density of states matrix at the tip atom. The advanced Green's function, $\hat{g}^A_{ni}(E)$, describes the electron propagation from an atom n at the surface down to the atom i, closing the loop to give the current between atoms j and i. The summation runs over all tunneling active atoms in the sample surface, m and n. The energy integration is performed between the Schottky barrier (eV_o, assumed to be 0.66 eV [4]) and the applied voltage (eV). However, due to the exponential energy dependence of the coupling matrices, T_{m0}, T_{0n}, the integrand is a strongly increasing function with energy, so that already the contribution at the highest energy (eV) provides the dominant fraction of the elastic BEEM current in the near threshold region. To elucidate the physics behind the observed effects, the presented results will therefore be restricted to this highest energy.

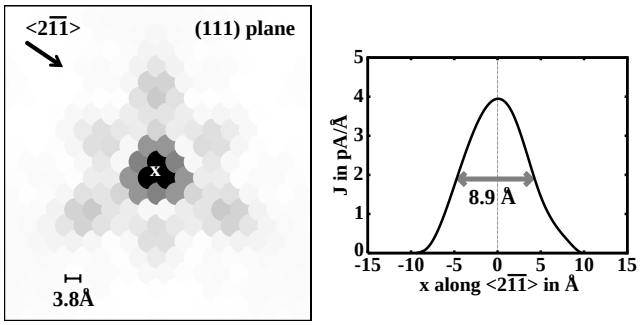

FIG. 1. Current distribution in a Si2 layer parallel to the surface after propagation through 30Å $CoSi_2$(111) film. Injection from the tip at $1.5eV$ occured in the center of the shown plane (white X), where the maximum current propagating in a focused beam along the <11$\bar{2}$> direction can still be found. The linear gray scale indicates current intensity at each atomic site: black maximum to white zero current. The right hand panel displays a cut through the focused beam in <2$\bar{1}\bar{1}$> direction from which a FWHM of 8.9Å can be derived.

With Eq. (1), the elastic propagation of electrons in real space from the tip down to the M-S interface can be followed. In order to obtain the final BEEM current, we further need to calculate the momentum distribution of the electrons that reach the M-S interface, $J_I(E, \mathbf{k}_\parallel)$. This momentum distribution can be expressed as [9]:

$$J_I(E, \mathbf{k}_\parallel) = \frac{4e}{\hbar} \Im \, Tr \sum_b \left[\hat{T}_{bc} \hat{g}^R_{c1} \hat{T}_{10} \hat{\rho}_{00} \hat{T}_{01} \hat{g}^A_{1b} \right], \quad (2)$$

where in this case $\hat{g}^R_{c1}(E, \mathbf{k}_\parallel)$ is the retarded Green's function for the unperturbed metal, linking layer c (the metal layer at the M-S interface) and the surface layer 1 which is connected to the tip by a hopping matrix $\hat{T}_{10}(\mathbf{k}_\parallel)$. $\hat{T}_{bc}(\mathbf{k}_\parallel)$ is the hopping matrix connecting all upper layers b with the interface layer c and finally $\hat{g}^A_{1b}(E, \mathbf{k}_\parallel)$ is the advanced Green's function linking the surface layer with layer b. These advanced and retarded Green's functions and the ones appearing in Eq. (1) can be readily computed using renormalization group techniques [10].

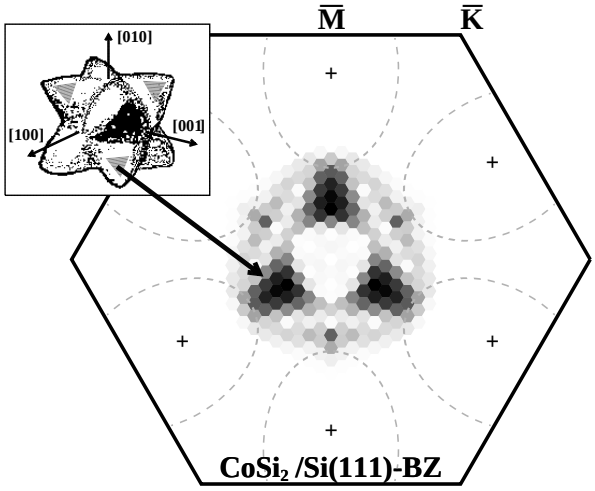

FIG. 2. Electronic current distribution in the 2D interface Brillouin zone, $J_I(E, \mathbf{k}_\parallel)$, evaluated at 1.5eV after 30Å film propagation. The current intensity is drawn with a linear gray scale, black representing maximum current. Also shown are the ellipsoids defining available states in the semiconductor below 1.5 eV. The inset contains the constant energy surface sheet mainly responsible for the current propagation: the shaded flat terraces point in <11$\bar{2}$> direction and correspond to the dark areas of the 2D current distribution.

First of all, we apply our formalism to the case of a $CoSi_2$(111)-(1x1)Si-rich surface terminated film [11] and analyze the propagation of electrons from the tip to the $CoSi_2$/Si(111) interface in real space. In the <111> direction, this metal may be characterized by a stacking sequence of Si1-Co-Si2 trilayers (cf. Fig. 3a) with the interface to Si mainly formed below a Si2-type layer [11]. Fig. 1 shows the current distribution on every atom in such a Si2 layer 30Å below the surface as to compare with experiments performed on films of equal width [4]. The prominent effect we deduce from this figure is that the electrons injected into the silicide are focused inside a very narrow beam propagating perpendicular to the film. The right hand panel in Fig. 1 shows the intensity in real space along a line in <2$\bar{1}\bar{1}$> direction through the center of the beam: the obtained FWHM of 8.9Å compares

very well with the resolution of ≈ 10.0Å with which interface point defects could be resolved experimentally in such films [4]. This, up to now, highest achieved spatial resolution with BEEM had been impossible to explain assuming free electron propagation inside the metal, predicting beam widths of 25 Å for the same distance.

The electron focalization is due to the particular shape of the constant energy surface sheet responsible for the major current propagation (see inset of Fig. 2); it can be shown that between E_F and $E_F + 2.5$ eV these sheets are practically the same except by a uniform shrinkage that increases linearly with energy. The shaded regions are nearly flat terraces perpendicular to the $<111>$ direction, and act as a kind of "condenser lens" on the electron beam, keeping the electrons with corresponding $\mathbf{k}$-vector propagating along the $<111>$ direction [3]. This reasoning is complementary to the current distribution we have calculated in $\mathbf{k}_{\|}$-space using Eq. 2 and shown in Fig. 2. The three dark regions of the 2D Brillouin zone where the $\mathbf{k}_{\|}$-current is mainly concentrated correspond to the flat areas of the constant energy surface.

The onset of BEES I(V) characteristics is linked to the Schottky barrier height between the metal and the semiconductor. In our calculations that onset appears at 0.9eV, 0.24eV larger than the Schottky barrier height commonly accepted for the $CoSi_2$-Si interface [12,13]. This is related to the assumed $\mathbf{k}_{\|}$-conservation and to the absence of states in the metal matching the conduction band minima in the semiconductor. The same delayed onset has been obtained by Stiles and Hamann [14], and it has been argued [13,15] that a smaller onset can appear if a non $\mathbf{k}_{\|}$-conserving scattering process is operative for the injected electrons at the silicide-silicon interface. Indeed, the results reported by these authors for $CoSi_2$/Si(111) seem to point out that the effect of such processes is to modify only slightly the BEEM-current beyond 0.9 eV, but is enough to yield the appropriate M-S barrier height at ≈ 0.66 eV. Therefore, for energies larger than 0.9 eV, current injection conserving $\mathbf{k}_{\|}$ dominates the spectra, as expected intuitively from the good matching between the Si and $CoSi_2$ lattices, and our theory applies. We should also mention, however, that non $\mathbf{k}_{\|}$-conserving processes must play an important role for the BEEM contrast of defect images at the M-S interface due to the nanometric size of the electron beam.

In our next step we consider the case of the (2×1) surface structure of $CoSi_2$/Si(111). Stalder et al. [16] reported this Si-rich reconstruction for $CoSi_2$(111) with a geometry very similar to Pandey's π-bonded chain model [17]. Fig. 3a shows a sideview of this surface geometry with its topmost Si-bilayer reconstructed in alternating high and low chains. We have analyzed how the geometry of the reconstructed (2×1) surface modifies the electron focalization discussed above for the (1×1) surface. The main effect of the reconstruction is to broaden the FWHM of the focused beam to 13.6Å. This effect, that we associate to a larger area of the surface unit cell where the tunneling electrons are injected, has also been observed experimentally by Sirringhaus et al [4].

A very interesting result observed for this reconstruction is that in the constant-current STM mode, the BEEM image of the interface reflects the atomic surface periodicity, but out of phase with the topographic corrugation [5]. This BEEM anticorrugation has previously been attributed to atomic-scale variations of the energy tunneling distribution of the injected electrons [5]. In order to analyze these results, we calculate the current that reaches the M-S interface as a function of the tip position for a constant tunneling current (1 nA). In general, to compute the BEEM current injected into the semiconductor we would need to use a transmission coefficient, $T(E, \mathbf{k}_{\|})$, determined from the matching of states at the interface. However, this is not necessary to study the particular dependence of the BEEM current on the tip position, as T is independent of the tunneling injection. Moreover, we have found that the $\mathbf{k}_{\|}$ distribution of the current is nearly the same for all the different positions of the tip, in accordance with the conclusions raised in [5]. Therefore, to study the effect that the surface reconstruction introduces in the BEEM current we can simply analyze the total current reaching the interface. Fig. 3b shows that this quantity presents anticorrugation with respect to the one found in the surface reconstruction.

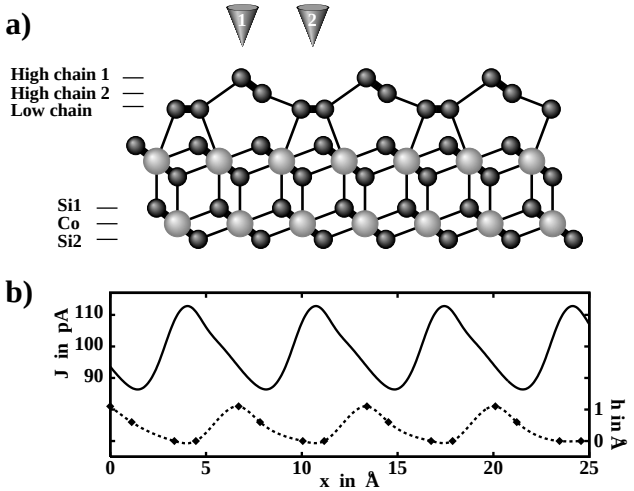

FIG. 3. a) Sideview of the (2×1) surface reconstruction with tip positions 1 (high chain injection) and 2 (low chain injection). b) M-S interface current at 1.5eV after 30Å film propagation as a function of the tip position (higher curve, left scale in pA). The lower curve gives a schematic surface topography along the scan line (right scale in Å).

To understand the physics behind this effect, we have studied the injected current along the different metal layers. Fig. 4 shows our results for the tip located either on the highest or on the lowest position on the reconstructed surface (points 1 and 2 of Fig. 3a). Two important conclusions can be drawn from our results: first, the injected

current along the metal layers is damped by the introduction of an imaginary component for the energy, $E + i\eta$, that simulates the electron-electron scattering processes (in our case we have used $\eta = 0.05$eV, that yields attenuation lengths in accordance with experimental data [18]); only at long distances this damping results in an exponential behaviour for the current. Second, at short distances the current presents a faster decrease associated with the injection of electrons along surface states channels. As Fig. 4 shows, in the (2×1) reconstruction the current decreases by 65% after the electrons cross the first two Si-layers and the first $CoSi_2$ trilayer (where surface states are mainly localized). This is the effect of having the injected electrons propagating also along the surface bands, departing in this way from the bulk states channels that contribute to the current propagating across the metal layers.

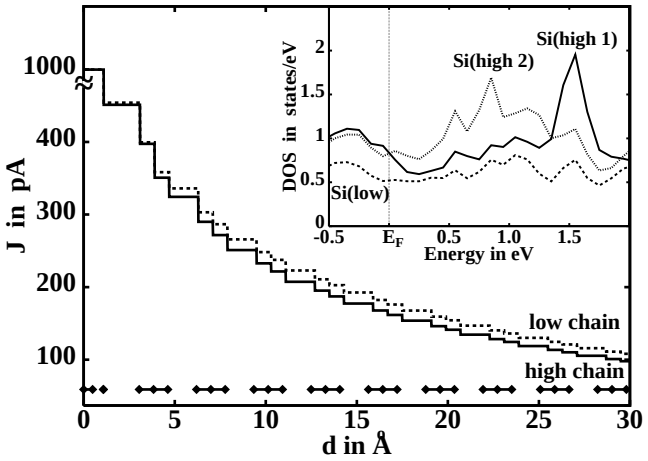

FIG. 4. Current across the first 30Å of the silicide film at 1.5eV after injection on a high chain (solid line) or on a low chain (dotted line). The diamonds at the bottom indicate the trilayer Si1-Co-Si2 sequence of $CoSi_2$ in the (111) direction, with the final reconstructed Si chain-bilayer. The inset shows the surface density of states projected on the high and low chain atoms in the energy region important for BEEM.

The anticorrugation obtained in Fig. 3b for the total current arriving at the M-S interface can be understood in terms of this role played by the surface states. These states have larger weights on the atoms of the higher chains than on the low chain ones as we can see in the surface density of states shown in the inset of Fig. 4. Therefore, for those tip positions in which electrons are injected predominantly into high chain atoms, there is a larger probability for having those electrons propagating along surface states channels than the one obtained for injection on the low chain atoms. Consequently, in the usual experimental constant-current STM mode, less current crossing the metal layers and reaching the interface remains. This difference with respect to the current injection, which stays almost constant after crossing the first $CoSi_2$ trilayer (5Å), explains why the BEEM image shows anticorrugation with respect to the surface topography. Note, however, that the absolute order of magnitude of this effect depends strongly with energy: as shown in Fig. 3b, the anticorrugation contrast is 25% for 1.5 eV and a lower contrast is obtained for larger voltages. This dependence is related to the fact that surface states are concentrated rather close to the Fermi level.

In conclusion, we have presented a theoretical analysis of the propagation of an electron beam injected in a $CoSi_2(111)$ crystal using a STM tip. Our results show conclusively that the silicide electronic band structure plays a central role in the focalization of the electron beam. This behaviour and the specific $\mathbf{k}_{\|}$-contribution to the current have been associated with flat terraces of the constant energy surface producing a *condenser lens* effect on the electron propagation. Our results explain the high resolution observed in real space for BEEM experiments performed on $CoSi_2$/Si(111) interfaces. Additionally, we have also shown how the BEEM current can map out the silicide surface reconstruction due to the role played by the localized $CoSi_2(111)$-(2x1) surface states on the current injected from the tip.

We acknowledge financial support from the Spanish CICYT under contracts number PB97-1224 and PB92-0168C. K.R. and K.H. are grateful for financial support from SFB292 (Germany).

[1] W.J. Kaiser and L.D. Bell, Phys. Rev. Lett. **60**, 1406 (1988); L.D. Bell and W.J. Kaiser, Phys. Rev. Lett. **61**, 2368 (1988).
[2] For comprehensive reviews see M. Prietsch, Phys. Rep. **253**, 164 (1995); L.D. Bell and W.J. Kaiser, Annu. Rev. Mater. Sci. **26**, 189 (1996).
[3] F.J. Garcia-Vidal, P.L. de Andres, and F. Flores, Phys. Rev. Lett. **76**, 807 (1996); P.L. de Andres et al., Phys. Scr. **T66**, 277 (1996).
[4] H. Sirringhaus, E.Y. Lee, and H. von Känel, Phys. Rev. Lett. **73**, 577 (1994); T. Meyer and H. von Känel, Phys. Rev. Lett. **78**, 3133 (1997).
[5] H. Sirringhaus, E.Y. Lee, and H. von Känel, Phys. Rev. Lett. **74**, 3999 (1995); H. Sirringhaus, E.Y. Lee, and H. von Känel, Surf. Sci. **331/333**, 1277 (1995).
[6] H. von Känel, Th. Meyer, and H. Sirringhaus, Journal of Crystal Growth **175/176**, 340 (1997).
[7] S. Sanguinetti et al., Phys. Rev. B **54**, 9196 (1996).
[8] L.F. Mattheiss and D.R. Hamann, Phys. Rev. B **37**, 10623 (1988).
[9] K. Reuter et al., Phys. Rev. B, *in press*.
[10] F. Guinea et al., Phys. Rev. B **28**, 4397 (1983).
[11] U. Starke et al., Surf. Rev. Lett. **5**, 139 (1998).
[12] J.Y. Duboz et al., Phys. Rev. B, **40**, 10607 (1989).
[13] H. Sirringhaus et al., Phys. Rev. B **53**, 15944 (1996).

[14] M.D. Stiles and D.R. Hamann, J. Vac. Sci. Technol. B **9**, 2394 (1991).
[15] W.J. Kaiser et al., Phys. Rev. B **44**, 6546 (1991).
[16] R. Stalder et al., Surf. Sci. **258**, 153 (1991).
[17] K.C. Pandey, Phys. Rev. Lett. **47**, 1913 (1981).
[18] E.Y. Lee et al., Phys. Rev. B **52**, 1816 (1995).